Meteoritics & Planetary Science 38, Nr 12, 1865–1875 (2003)
Abstract available online at http://meteoritics.org

Mineralogy, microtexture, and composition of shock-induced melt pockets in the Los Angeles basaltic shergottite

Erin L. WALTON* and John G. SPRAY

Planetary and Space Science Centre, Department of Geology, University of New Brunswick
2 Bailey Drive, Fredericton, New Brunswick E3B 5A3, Canada
*Corresponding author. E-mail: j5rng@unb.ca

(Received 20 February 2003; revision accepted 19 December 2003)

Abstract–Analytical electron microscopy of shock features in the basaltic shergottite Los Angeles (stone 1) reveals: 1) shock recorded in the bulk sample; and 2) localized pressure and temperature excursions that have generated melt pockets up to 4 mm in diameter. Bulk shock effects include microfaulting (offsets 1–200 μm), mosaicism, deformed exsolution lamellae and planar fracturing in pyroxene, undulose extinction in whitlockite, mechanical twinning in titanomagnetite and ilmenite, and the transformation of plagioclase to maskelynite (≤4% remnant reduced birefringence). The pressure estimates for bulk shock are 35–40 GPa. Localized shock excursions have generated three types of discrete melt zones (0.07 × 1.3 mm to 3.0 × 3.5 mm apparent diameter) possessing glassy to microcrystalline groundmasses. These melt pockets are differentiated on the basis of size, clast volume, and degree of crystallization and vesiculation. Melt veins and melt dikelets emanate from the melt pockets up to 3 mm into the host rock but do not necessarily connect with other melt pockets. The melt pockets were generated by pressure-temperature excursions of 60–80 GPa and 1600–2000°C, resulting in discrete melting of adjacent host rock minerals at grain boundary margins. Concentric zoning in the margins of clinopyroxenes coincides with a progressive reduction in birefringence as melt pockets are approached. This suggests that the shock excursions were focused as point sources in the wake of the shock front that induced bulk damage.

INTRODUCTION

Los Angeles is a basaltic shergottite, comprising two relatively unweathered stones (stone 1, 452.6 g; stone 2, 245.4 g), recovered from the private rock collection of Robert Verish in 1999 (Rubin et al. 2000). Rb-Sr and Sm-Nd radiometric ages of the meteorite are 165 ± 11 and 172 ± 8 Ma, respectively, with a preferred age of 170 ± 8 Ma (Nyquist et al. 2001). This young radiometric age falls within the range of 165–475 Ma for other basaltic and lherzolitic shergottites, interpreted as the timing of magmatic crystallization (McSween 2002). An ejection age of ~3 Ma suggests that Los Angeles was launched from the martian surface at the same time as the basaltic shergottites QUE 94201, Shergotty, and Zagami (Garrison and Bogard 2000; Nishiizumi et al. 2000; Terribilini et al. 2000).

This work describes the microtexture and composition of shock-induced melt pockets in Los Angeles 7058 (hereafter referred to as Los Angeles). Two polished thin sections of stone 1 have been investigated using analytical electron microscopy. Studies of shock metamorphism in SNC meteorites help to constrain launch conditions in the context of the martian impact process and furthers our understanding of the origin of extreme shock excursions.

SAMPLES AND ANALYTICAL PROCEDURES

Two polished thin sections of Los Angeles stone 1 (7058-2, 2.1 cm × 1.2 cm; 7058-5, 1.3 cm × 1 cm) were obtained from the Smithsonian Institution for study. They are part of a group of serially sectioned slices made from a ~20 g slab through the approximate center of the stone, which was donated to the Smithsonian Institution by Robert Verish. Melt pockets and their host minerals in the 2 polished thin sections of Los Angeles were investigated using a JEOL 6400 digital scanning electron microscope (SEM) equipped with a Link Analytical eXL energy dispersive spectrometer (EDS) fitted with a Si (Li) LZ-4 Pentafet detector. Count times were 100 sec per analysis at beam operating conditions of 15 kV and 2.5 nA at a working distance of 39 mm. SEM backscattered electron imagery (BEI) was used to investigate the microtextures and mineralogy of the meteorite,

accompanied by the single spot analysis of individual minerals. Where alkali mobility was not deemed problematic, certain clast minerals were analyzed using a JEOL 733 electron microprobe equipped with 4 wavelength dispersive (WDS) spectrometers. The accelerating voltage was 15 kV with a 30 nA beam current, and the approximate beam diameter was 1–2 μm. Both analytical SEM and microprobe data and images were collected at the University of New Brunswick. Additionally, high resolution images were obtained at the JEOL Laboratory in Peabody, MA using a JEOL 6500F field emission gun scanning electron microscope (FEG-SEM). This was equipped with an In-Lens Thermal FEG, which produces a probe current sufficient for WDS and EDS. Photomicrographs were taken with an accelerating voltage of 15 kV and a 5 nA beam current at a working distance of 10 mm.

Raster scanning was used to determine the approximate bulk chemistry of the melt pockets. Crystallites and normal (non-diaplectic) glasses were rastered in separate areas of 20 μm by 26 μm, at 5000× magnification. EDS was used instead of WDS because it not only enables rapid, simultaneous major element analysis but also operates at lower beam currents than WDS. This minimizes thermal excitation and charge effects and, hence, alkali metal migration (e.g., Spray and Rae 1995). Lithic and crystal fragments, derived from host rock minerals adjacent to the melt pockets, were excluded from bulk melt pocket analysis. Identification of lithic and crystal fragments was based on the presence of reaction rims, subrounded/rounded morphologies resulting from thermal corrosion, a high density of irregular fractures within clasts (typically containing injections of remobilized Fe-sulfides and melt material), and/or the presence of abundant dendritic crystallites that nucleated at xenocryst margins.

HOST MINERALOGY

Los Angeles is igneous textured and dominated by relatively coarse-grained (2–4 mm) anhedral to subhedral clinopyroxene (ferroaugite) and subhedral to euhedral plagioclase (now maskelynite). It is, thus, a microgabbro, probably having formed within the core of a thick (several meter) lava flow or as a near-surface feeder to basaltic extrusives. Los Angeles has a ferroan bulk composition, a lower bulk MgO than any other known martian meteorite, enriched concentrations of incompatible elements, and a high abundance of late-stage phases. As such, Los Angeles is the most differentiated basaltic shergottite yet discovered (Rubin et al. 2000; Warren et al. 2000). A modal analysis (in vol%) of stone 1, given by Rubin et al. (2000), yields maskelynitized plagioclase (44.8%) and pyroxene (43.7%), with subordinate amounts of silica (2.4%), titanomagnetite (2.1%), fayalite (1.9%), K-rich feldspathic glass (1.6%) and merrillite/whitlockite (1.5%), accessory chlorapatite (0.9%), ilmenite (0.3%), and pyrrhotite (0.6%), and rare baddeleyite, pentlandite, and hercynitic spinel.

SHOCK EFFECTS

The shock damage in Los Angeles (summarized in Table 1) is manifest as: 1) effects recorded in the bulk sample; and 2) localized temperature and pressure excursions.

Bulk Shock Effects

A brief description of bulk shock effects in Los Angeles, based largely on optical observations, is given by Rubin et al. (2000). They note the transformation of plagioclase to maskelynite, deformed exsolution lamellae, mosaicism and

Table 1. Shock effects recorded in various mineral constituents of Los Angeles.[a]

Bulk rock constituents								
Shock effect	Plagioclase	Pyroxenes[b]	Whitlockite	Ti-Magnetite	Ilmenite	Pyrrhotite	Fay + aug + sil[c]	Si, K glass[d]
Reduced birefringence	±	(±)	(+)	–	–	–	–	–
Diaplectic glass	+							
Undulose extinction	±		±	–	–	–	–	–
Mosaisicm		(+)		–	–	–	–	–
Fracturing	(±)	(+)	(+)	(+)	(+)	(+)	(+)	(+)
Planar elements		+						
Mechanical twins				(±)	(±)			
Melt pocket								
Localized melting	+	+	+	+	+	+	+	
Present as quench crystallites	+	+	+	+	±		+	
Present as clasts within melt pockets	±	±	+	+	+			+

[a]+ = shock effects that are commonly observed; ± = shock effects that are rarely observed; ( ) = shock effects that increase in intensity approaching areas of localized melting; – = shock effect doesn't apply to specified mineral/phase.

[b](Ferro) augite, pigeonite.

[c]Pyroxferroite breakdown material (fayalite + Fe-augite + silica symplectic intergrowth).

[d]Silica and K-rich alkali symplectic glasses.

planar fracturing of clinopyroxene, pyrrhotite veins within clinopyroxene, polycrystallinity in some pyrrhotite grains, and a 350 μm-long microfault with ~15 μm displacement. Nyquist et al. (2001) report peak shock equilibration pressures for Los Angeles of 35–40 GPa, which fall within the proposed launch window for martian meteorites (Melosh 1984, 1985).

In this study, we also observe mechanical deformation manifest as microfaulting (with observed offsets of 1–200 μm), mosaicism, deformed exsolution lamellae and planar fracturing of pyroxenes, undulose extinction of whitlockite, and mechanical twinning in ilmenite and titanomagnetite. Maskelynite grains display radiating fractures that emanate from their outer margins into neighboring minerals (typically pyroxene), a feature noted by Chen and El Goresy (2000) for maskelynite in Zagami, Dar al Gani 476, and ALH 84001. Strongly reduced birefringence has been observed in rare grains of maskelynite, a feature also noted by Rubin et al. (2000). The majority (96%) of plagioclase in Los Angeles is completely isotropic. Xirouchakis et al. (2002) report weak plagioclase peaks in at least one grain analyzed by synchrotron X-ray diffraction, indicating that a small proportion of the crystalline structure has survived. Reduced birefringence at the edges of rare grains indicates that the plagioclase ($An_{46–64}Ab_{30–46}$) in Los Angeles is just beyond the transition from partially isotropic to fully isotropic.

Localized Shock Effects

Localized regions of melting comprise <1% of the meteorite by volume, forming self-contained (within the 2 dimensions of the thin section) melt pockets, melt veins, and melt dikelets.

Under the optical microscope, melt pockets appear as irregularly-shaped dark brown to black enclaves (Figs. 1a and 1b). They are commonly spatially related to large open fractures infilled with secondary terrestrial carbonates (Rubin et al. 2000). Calcite is also observed lining the inner cavities of vesicles within the melt pockets. Color variations, at higher magnification, consist of light brown, dark brown, and colorless flow-layered glasses in the larger melt pockets (as compared to smaller, microcrystalline melt pockets that are essentially opaque). Schlieren is used here to describe a layer in the melt pocket glass that is either texturally distinct from the surrounding glass and/or is compositionally distinct from surrounding glass. SEM analyses reveal that the dark brown schlieren are due to an abundance of small (≤0.5 μm) inclusions of Fe-sulfides and idiomorphic titanomagnetite grains (≤1 μm), while light-brown schlieren are devoid of them (both light and dark brown variants are otherwise compositionally similar, having approximate pyroxene composition). Colorless schlieren are normal (non-diaplectic) plagioclase glass that have incompletely mixed/homogenized with other coexisting silicate and sulfide melts. The colorless plagioclase glasses are, like light brown schlieren, free of minute Fe-sulfides and Ti-magnetite crystals. The composition of plagioclase schlieren lies within the range of those obtained for host rock maskelynite (Table 2).

Host phase ferroaugite and ferropigeonite bordering the melt pockets show reduced birefringence, grading, in some cases, to partial isotropism (Figs. 1a–1c). These effects are restricted to the side of the grain located adjacent to the melt pocket. In plane polarized light, the rims typically appear dark brown and blackened with proximity to the melt zone. Pyroxenes with $\delta = 0.012–0.015$ at the interior of the grain show birefringence reduced to $\delta = 0.007–0.000$ at the margin. Additionally, the zones are commonly concentrically arranged. SEM studies have revealed, for 3 pyroxene grains, a zone of reaction with the melt zone corresponding to those margins showing reduced birefringence in optical observations (Figs. 1c and 1d).

Three distinct types of melt pocket occur in the studied thin sections (Figs. 2 and 3):

1. Type 1: Microscopic (0.5 mm × 0.7 mm; 0.07 mm × 1.3 mm), vesiculated, clast-rich, with abundant crystallites (Fig. 2). X-ray compositional maps, obtained for a 3900 μm^2 area within a Type 1 melt pocket, show that crystallites are rich in Al, Si, and Ca (plagioclase). Entrained clasts are subangular and consist of isotropic and partially birefringent whitlockite and clasts comprising a symplectic intergrowth of alkali- and silica-rich glass. The clast sizes range from 0.5 to 200 μm (average = 39 μm; n = 100). Type 1 melt pockets are devoid of spheres of immiscible Fe-sulfide (pyrrhotite). The contact with adjacent host rock minerals varies from smooth boundaries to intrusive stringers and veins of melt material. Isolated wisps and stringers of melt material within maskelynite have also been observed in the immediate vicinity of the melt pocket. One such melt pocket contains clasts that display interior quench textures (Fig. 2f). Pyroxene compositions are almost

Table 2. Range in chemical composition (wt% oxide) for maskelynite and plagioclase schlieren.

	Maskelynite			Schlieren		
Wt%	avg	min	max	avg	min	max
SiO_2	55.8	53.5	58.8	57.0	54.4	59.5
Al_2O_3	27.1	25.6	28.7	25.4	23.6	28.5
FeO[a]	0.7	0.5	0.8	1.1	0.2	1.9
CaO	10.1	7.9	11.8	8.8	6.8	11.8
Na_2O	5.4	4.3	6.5	5.7	4.6	6.6
K_2O	0.3	0.1	0.6	0.9	0.1	1.2
Total	99.2			98.8		
n[b]	32			14		

[a]Total Fe reported as FeO.
[b]Number of grains analyzed.

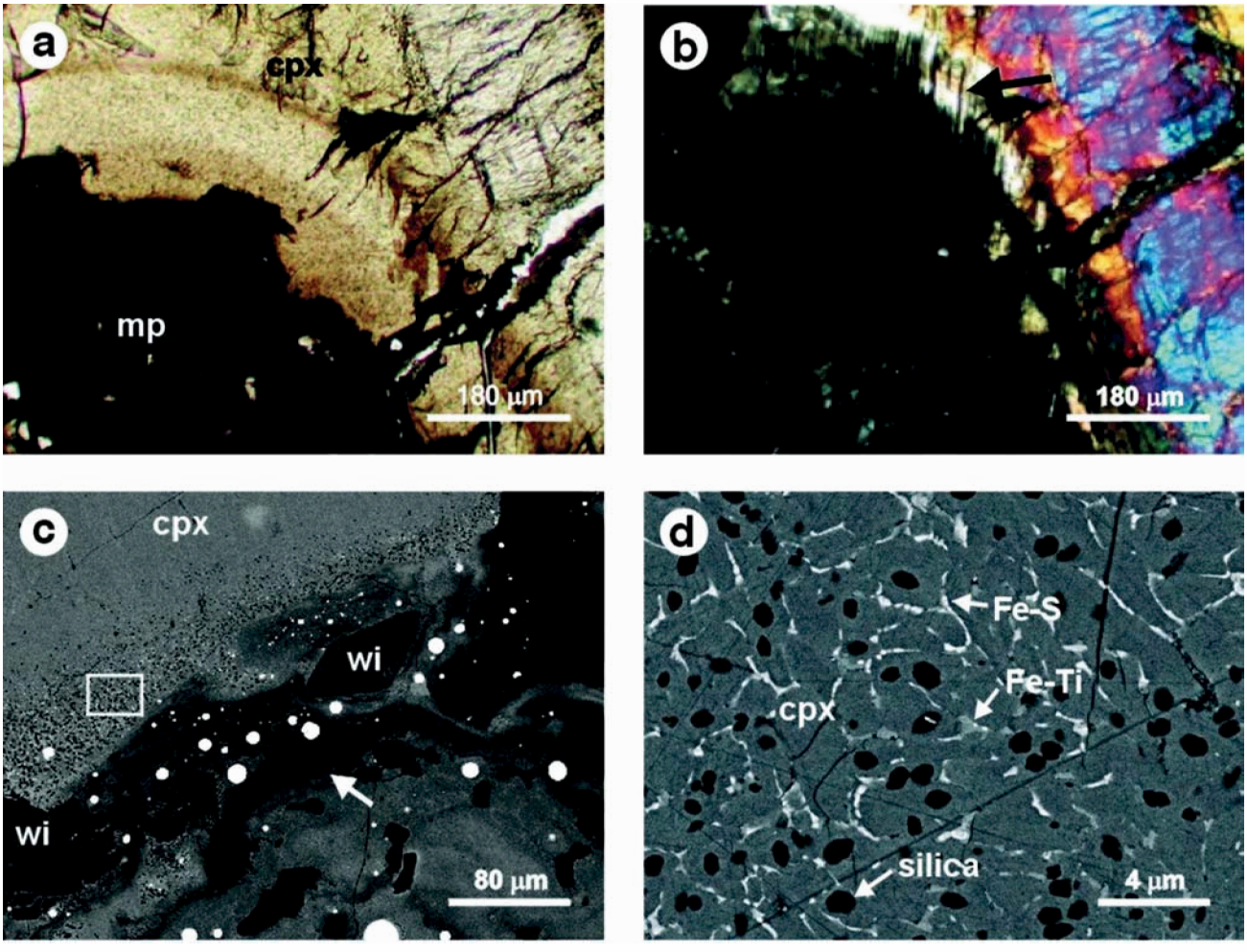

Fig. 1. a) and b): Optical photomicrographs of the contact between a host rock clinopyroxene grain (cpx) with a melt pocket (mp) in Los Angeles. Zoning in the pyroxene (obtained from microprobe point analyses) is complex but, overall, changes from a Mg-rich core to a Fe-rich rim. In plane polarized light (a), the margin adjacent to the melt pocket is "stained" a light-brown color arranged in concentric zones; b) crossed polars view of the same area shown in (a) revealing the marked change in birefringence from δ_{max} = 0.020–0.000 at the melt pocket margin. Deformed exsolution lamellae in the pyroxene are indicated by the black arrow; c) and d): backscattered electron images (BEI) of the same pyroxene as in (a) in contact with the melt pocket, rotated 90°; c) abundant fragments of whitlockite (wi) are located within the melt pocket, adjacent to the reaction zone. The arrow indicates plagioclase schlieren; d) reaction zone at the margin of cpx adjacent to the melt pocket showing the distribution of silica, pyrrhotite, titanomagneite, and pyroxene. The location is highlighted as a white box in (c).

exclusively manifest as normal glass within the smaller melt pockets; however, rare clasts have been observed at the melt pocket margins.

2. Type 2: Microscopic (0.03 × 0.4 mm), vesiculated, clast-poor, with abundant crystallites of idiomorphic to subidiomorphic silica crystals (with accessory Al_2O_3) embedded in an unresolvable glassy groundmass rich in Fe, Ca, and Na (Figs. 3a–3c). The groundmass is relatively pristine and shows no signs of devitrification or alteration to aggregates of new phases (e.g., clays, iddingsite). The interior of the melt pocket is coarser grained, fining toward the margin (Fig. 3d). Maskelynite adjacent to the melt pocket has recrystallized in a ~5 μm-wide rim surrounding the melt pocket. As with Type 1 melt pockets, Type 2 are also characterized by an absence of immiscible blebs of Fe-sulfides.
3. Type 3: Macroscopic (3.5 mm × 3.0 mm), dominantly vesicular, relatively clast-poor, with flow textures and abundant spheres/blebs of immiscible Fe-sulfides (Figs. 2a–2e). Sulfide spheres range from ≤0.1 to 20 μm in diameter and comprise mono- and polycrystalline pyrrhotite. Most vesicles are spherical, indicative of quenching at low confining pressure and low shear strain. Some are elongated with their c-axes parallel to the direction of flow. Vesicles range from ≥1 μm to 0.5 mm apparent diameter. Individual schlieren can be traced for several mm, yet their length and width are

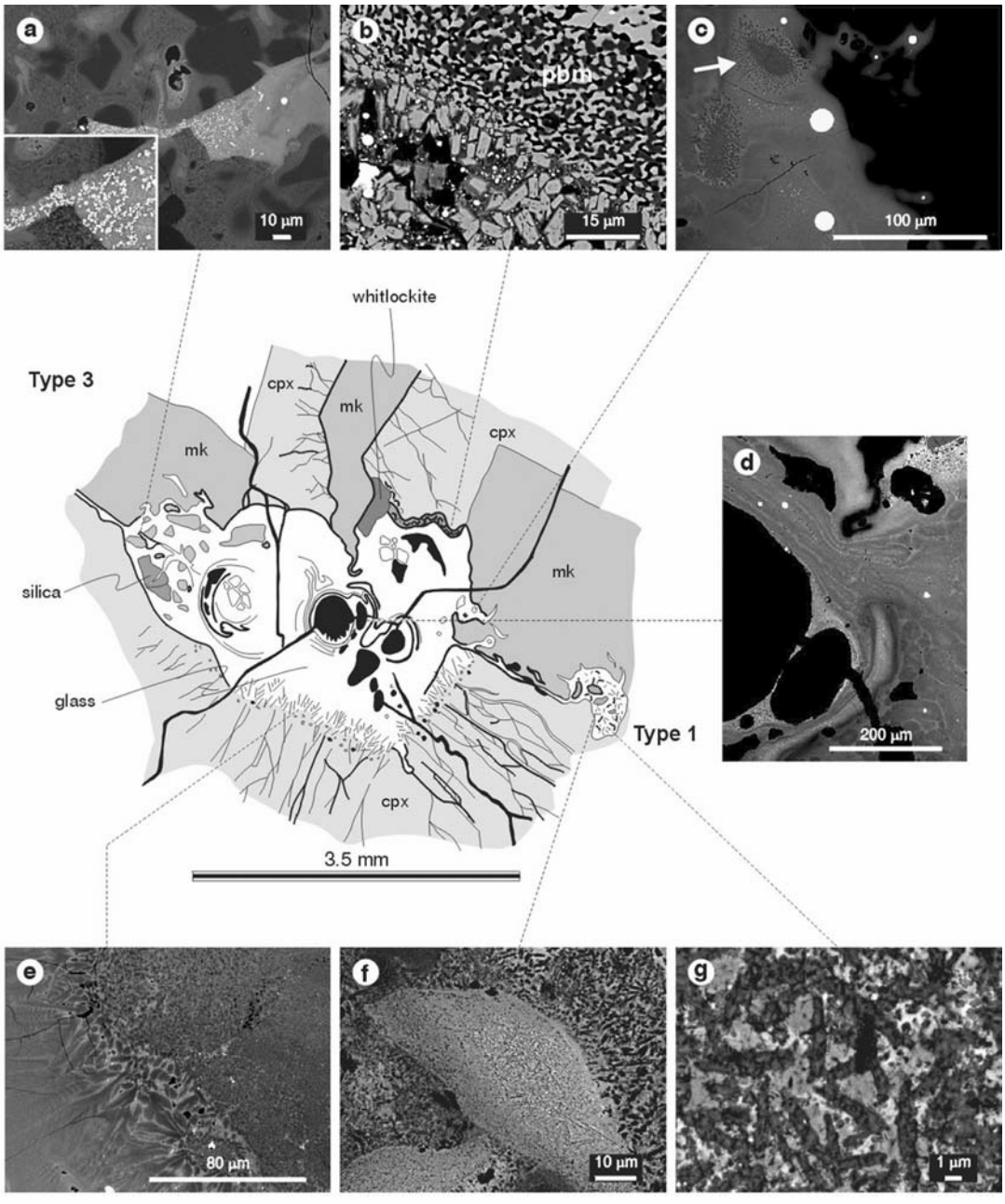

Fig. 2. Backscattered electron images of Type 3 (a–e) and Type 1 (f–g) melt pockets in context with host rock minerals maskelynite (mk) and clinopyroxene (cpx): a) crosscutting relationship between two coexisting silicate melts within one melt pocket (Type 3). The contact between the 2 melts is diffuse, indicating that the higher viscosity melt was relatively warm when the other was intruded. The higher viscosity melt contains abundant subidiomorphic crystals with square- and diamond-shaped cross-sections that increase in abundance with distance from the main melt pocket. Small crystal size prohibits quantitative analysis, but qualitative microprobe analysis indicates that only iron and titanium are present in proportions 3 to 1, suggesting titanomagnetite; b) the pyroxferroite breakdown material (pbm) with typical vermicular texture in the host rock (upper right hand side) changes to skeletal and feather fayalite crystals embedded in a glassy groundmass with pyrrhotite globules at the contact between host rock phases and the melt pocket; c) intrusive relationship between maskelynite (dark grey/black, right hand side) and the melt pocket. The white spheres are pyrrhotite. The cross-sections through quenched whitlockite needles embedded in the glasses are shown by the white arrow; d) glassy groundmass of a Type 3 melt pocket with compositionally distinct flow-layering (revealed by grey-scale variations in BEI imaging) and cellular texture of glasses (upper and lower right hand side). The two black subspherical structures at the bottom of the image are vesicles connected by an open, irregular fracture; e) dendritic crystallites of pigeonite and orthopyroxene nucleating at the edge of a host-rock pyroxene grain at the melt pocket margin; f) clast containing quench textures within a Type 1 melt pocket; g) microcrystalline groundmass typical of a Type 1 melt pocket containing abundant crystallites rich in Al, Si, and Ca (plagioclase).

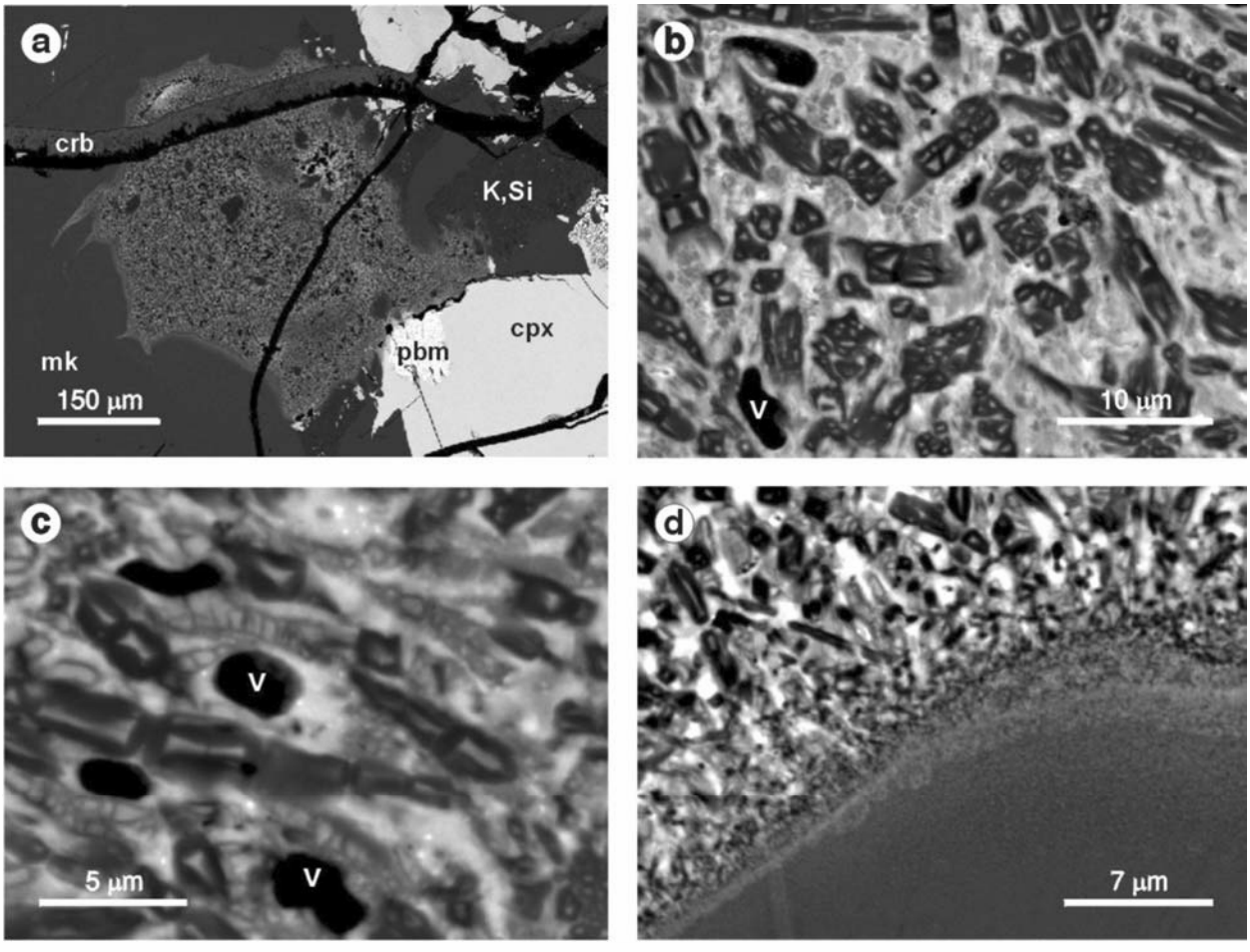

Fig. 3. Backscattered electron images of melt pocket Type 2 in Los Angeles: a) low magnification overview of melt pocket (center of photo). Host rock minerals adjacent the melt pocket are maskelynite (mk), clinopyroxene (cpx), an intergrowth of K-rich feldspathic glass and silica-rich glass (K, Si), and pyroxferroite breakdown material (pbm). Carbonates (crb) partially infill an E-W-trending fracture that crosscuts both host rock minerals and the melt pocket; b) higher resolution image of the interior of the melt pocket. Silica (with minor amounts of aluminium) forms subidioblastic to idioblastic crystals with roughly cubic-shaped cross sections. The vesicles (v) are irregularly-shaped; c) higher resolution cross-sections through the crystals depicted in (b) show unusual morphologies, like primate metatarsals. The interior of the crystals are compositionally similar to the groundmass, and are enriched in Fe, Mg, and Ca; d) contact between the melt pocket (top) and maskelynite (base of photo) is gradational, fining toward the margin. Maskelynite has recrystallized in a ~10 μm-wide rim in direct contact with the melt pocket.

highly variable. Contact relationships of individual schlieren with the surrounding glass range from sharp to highly diffuse. The schlieren show compositional variability attributed to melting of different proportions of minerals adjacent to the melt pockets (Tables 2 and 3). The proportion of locally derived lithic and crystal fragments increases toward the melt pocket margin. These consist of titanomagnetite, maskelynite, whitlockite, and alkali- and silica-rich glasses. Pyroxene has never been observed as clasts entrained in any of the large melt pockets.

Two distinct types of remobilized melt material emanate from the melt pockets (Fig. 1). They include thin (0.05–10 μm apparent thickness), non-vesicular, opaque and/or glassy veins (referred to as melt veins) and thicker (50–210 μm apparent thickness), vesicular, sinuous apophyses of melt material (referred to as melt dikelets). Melt veins comprise sulfide- and melt-filled fractures and microfaults with small lateral offsets (up to 80 μm). They possess discordant contacts with the host minerals, commonly form an interlocking network of anastomosing branches surrounding unmolten host rock constituents, and crosscut host rock minerals. Melt veins have not been observed to penetrate more than 550 μm from their source melt pockets (i.e., they do not completely transect the sample). A high concentration of melt veins induces a distinct darkening (opacity) of pyroxene grains in optical microscopy (referred to as "shock blackening" in chondrites; Stöffler et al. 1991).

Melt dikelets emanate from the main melt pocket and commonly enlarge to form subsidiary melt pockets. However,

some are observed to be wedge-shaped, wherein they taper off, typically within 3 mm from the source melt pocket. In contrast to the melt veins, they contain abundant vesicles and are confined to grain boundaries of relatively high and low density minerals. Contacts with adjacent minerals are diffuse. To observe stringers or blebs of melt co-mingling with adjacent host rock minerals is common.

While interconnected melt pockets do occur in Los Angeles, isolated pockets are more prevalent. Due to the highly irregular nature of typical shock veins (especially with increasing peak shock pressure; Stöffler et al. 1991), the tapering melt veins of Los Angeles possibly connect to seemingly isolated melt pockets out of the 2-dimensional plane of the thin section. However, melt veins in Los Angeles are morphologically distinct from typical discordant pseudotachylyte-like shock veins observed in other SNC meteorites (e.g., Shergotty; Stöffler et al. 1986) and ordinary chondrites (Stöffler et al. 1991) that commonly transect the whole meteorite.

In Los Angeles, the contact between the melt pockets and adjacent host rock minerals is irregular and commonly transitional (Fig. 1c). Host rock minerals adjacent to the melt pockets have been partially melted or recrystallized. The melt pockets, and melt veins and dikelets emanating from melt pocket margins, commonly crosscut both primary igneous textures and bulk shock effects.

Microscopic areas of alkali- and silica-rich glass (3.36–5.48 wt% K_2O, 1.59–3.37 wt% Na_2O, 87.9–97.5 wt% SiO_2, and 2.2–4.2 wt% Al_2O_3, respectively) are associated with maskelynite and silica crystals in the bulk sample. They range in apparent diameter from ~20–350 μm and exhibit a symplectic intergrowth texture between the two phases. Microfaults emanating from melt pocket margins displace the adjacent alkali- and silica-rich glasses (up to 15 μm). However, the alkali- and silica-rich glasses at the melt pocket margins contain entrained schlieren and globules of melt material that are detached from the melt pocket. The fluid nature of the material is indicated from the presence of pyrrhotite spheres and vesicles.

Regions of localized melting indicate a minimum melting temperature for nonporous basalts of 1600°C (Stöffler 1984). Additionally, melting of ilmenite indicates temperatures in excess of 1800°C (El Goresy et al. 1968). Localized pressure and temperature excursions within melt pockets, based on experimental data (Keiffer et al. 1976; Stöffler 1984; Schmitt 2000), are estimated at 60–80 GPa and 1600–2000°C, respectively. Schaal and Hörz (1977) observed melting of pyroxene in experimentally shocked basalts at a minimum pressure limit of 80 GPa.

Quench Crystals

One feature common to all melt pockets in Los Angeles is the presence of quench crystals. The crystals have a variety of distinctive shapes (skeletal, dendritic, feathery) and they comprise a variety of minerals (olivine, whitlockite, titanomagnetite, plagioclase). Quench crystals are invariably microscopic. Severely fractured, melt-intruded clinopyroxenes adjacent to the melt pockets allow for preferential nucleation of dendritic crystals that extend from the contact into glass. These consist of intimate intergrowths of ferropigeonite ($Fs_{73}En_{18}$) and orthopyroxene ($Fs_{40}En_{52}$) with dendritic textures (Fig. 2e). In addition, crystal fragments within melt pockets, locally derived from adjacent host minerals, serve as nucleation sites for dendritic growth (Fig. 4). These textures are consistent with rapid diffusion-controlled crystal growth from the melt (Kirkpatrick 1975).

Two melt pockets in Los Angeles show the symplectic intergrowth fayalite + ferroaugite + silica, a late-stage mineral assemblage resulting from the breakdown of pyroxferroite

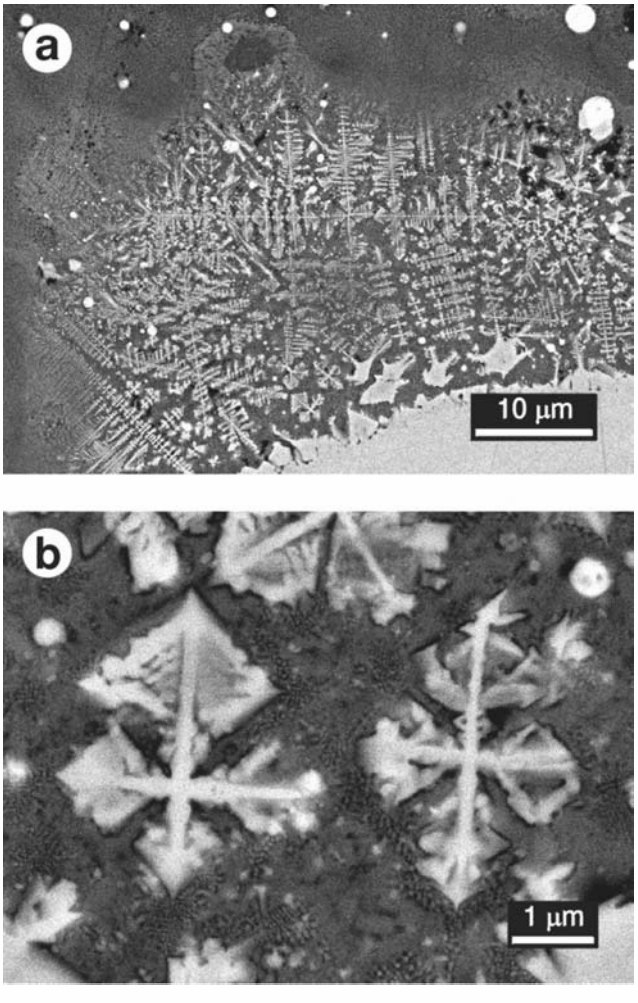

Fig. 4. Backscattered electron images of Los Angeles; a) a large titanomagnetite clast (lower right) within a melt pocket has seeded preferential nucleation of titanomagnetite crystallites with dendritic morphologies attesting to rapid cooling; b) higher magnification of the titanomagnetite crystallites are depicted in (a).

(Rubin et al. 2000), in direct contact with the melt pocket. At the melt pocket margin, the vermicular to microgranulitic texture, typical of the symplectites, changes to one of skeletal fayalite (Fa_{96}) embedded in a glassy matrix rich in Fe, Mg and Ca, and Fe-sulfide spherules (Fig. 2b). Numerous fractures in the vicinity of the melt pocket radiate from the contact with the melt into the fayalite + ferroaugite + silica intergrowth, causing microfaulting.

MELT POCKET COMPOSITIONS

The bulk chemistries of four melt pockets in Los Angeles are presented in Table 3. The compositions are variable from one pocket to another. CIPW norm calculations reveal that the melt pockets can be derived by fusing different mixtures of the host minerals dominated by plagioclase and pyroxene. Melt pocket 1 (Type 1) is dominated by normative quartz, orthoclase, plagioclase, and hypersthene; melt pocket 2 (Type 2) by quartz, orthoclase, plagioclase, and hypersthene; (Type 3) by mainly plagioclase, diopside, and hypersthene; melt pocket 4 (Type 3) by plagioclase, hypersthene, and apatite (whitlockite). Melt pocket compositions depend on which bordering host minerals contribute to melting and the proportion of melting of each phase (e.g., some melt pockets occur at the grain boundary of pyroxene and maskelynite, thus, these are the main components contributing to the melt). The occurrence of at least two coexisting silicate melts within one Type 3 melt pocket is revealed by crosscutting relationships (Fig. 2a). The more siliceous melt of the two (average 65 wt% SiO_2 obtained by raster scans, n = 8) is located in proximity to the melt pocket margin. This melt contains lithic and crystal fragments (~50%) of locally-derived silica and maskelynite. The less siliceous (average 43 wt% SiO_2 obtained by raster scans, n = 6), lower viscosity melt crosscuts the former, tapering off to thin stringers (≤1 μm in apparent thickness). The shape of the overall melt pocket is roughly spherical (Fig. 2), i.e., no textural evidence exists to suggest that these crosscutting relationships are the result of two independently formed melt pockets. Although the two silicate melts were most probably subject to the same cooling rates, the abundance of lithic and crystal fragments would have increased the amount of heterogeneous nucleation sites, favoring more rapid crystallization concomitant with an increase in viscosity. This is also consistent with rapid crystallization in Type 1 melt pockets containing abundant clasts of host rock minerals (Figs. 2f and 2g).

DISCUSSION

Melt pockets within Los Angeles can be divided into 3 types based on size, clast volume, and degree of vesiculation.

Table 3. Bulk compositions of shock melt pockets (in wt%) for Los Angeles stone 1.

	Melt pocket 1 (Type 1)			Melt pocket 2 (Type 2)			Melt pocket 3 (Type 3)			Melt pocket 4 (Type 3)			
wt%	avg	min	max	avg	min	max	avg	min	max	avg	min	max	5[a]
SiO_2	58.9	51.1	69.1	62.7	58.5	73.1	45.7	36.5	53.5	32.8	25.5	46.7	49.1
Al_2O_3	9.5	12.0	0.6	14.4	11.9	18.3	4.2	1.7	9.1	3.3	1.5	4.6	11.2
TiO_2	0.5	0.3	0.6	0.3	0.2	0.5	1.5	0.4	4.6	1.1	0.5	1.1	1.30
FeO[b]	21.9	12.8	32.9	11.3	6	18.9	30.5	19.7	40.4	29.9	23.4	44.1	21.2
MnO	0.5	0.7	0.3	0.3	n.d.[c]	0.5	0.7	0.4	1.2	0.7	0.5	1.3	0.45
MgO	0.9	0.5	2.6	0.3	0.6	5.2	4.2	1.6	11.0	0.8	0.6	1.3	3.53
CaO	3.7	5.7	1.3	5.8	5.8	7.3	9.6	7.0	12.8	15.9	5.9	16.4	9.95
Na_2O	1.8	1.0	2.3	2.4	1.2	3	0.2	n.d.	1.1	0.5	0.1	0.9	2.22
K_2O	2.1	0.2	2.7	1.3	0.8	1.8	0.3	n.d.	0.5	0.4	0.5	0.6	0.24
P_2O_5	–	n.d.	0.5	–	n.d.	0.1	–	n.d.	4.9	11.1	8.9	26.5	0.66
SO_3	–	n.d.	0.8	–	n.d.	n.d.	n.d.	0.4	2.7	–	n.d.	1.9	–
Total	100.1			98.8			99.6			97.0			99.86
n[d]	32			30			38			24			
CIPW norm													
Quartz	14.4			22.6			1.9			0			
Orthoclase	12.4			7.8			1.8			2.5			
Albite	15.2			20.6			1.7			4.4			
Anorthite	11.7			25			9.8			5.8			
Diopside	5.4			3.7			24.9			0.7			
Hypersthene	39.8			19.9			53.4			57.2			
Olivine	0			0			0			0.6			
Ilmenite	1			0.6			2.9			2.2			
Apatite	0.2			0			3.6			27.2			

[a]Data from Rubin et al. (2000) obtained by Instrumental Neutron Activation Analysis.
[b]Total Fe reported as FeO.
[c]n.d. = element oxides below the detection limit of the electron microprobe.
[d]n = number of raster scans per melt pocket.

Smaller (<1 mm) pockets (Types 1 and 2) tend to be crystallite-rich, while larger (>1 mm) pockets (Type 3) tend to be clast-poor and exhibit flow-structured glasses. Optically, shock effects are manifest as dark brown to black glassy and/or microcrystalline enclaves of melt material, melt veins, and deposits of sulfides and melt injected into fractures within silicates. In total, these localized regions of melting comprise <1 vol% of Los Angeles, and they are heterogeneously distributed throughout the sample.

Melt pockets invariably develop at the grain boundaries of minerals with contrasting shock impedance (shock wave velocity multiplied by the mineral's density), e.g., plagioclase and pyroxene. This is most obvious in smaller (≤1 mm) melt pockets (Type 1 and 2) where the original grain positions and boundaries are preserved. With increasing volume of melt, the original grains and their boundaries become obscured or destroyed. Typically, minerals adjacent to the melt pockets have smooth, arcuate margins at the contact with the melt. The composition of the melt pockets corresponds to localized melting of bordering host rock minerals. Melt veins have been observed to form an interlocking network of complex, anastomosing branches surrounding unmolten host rock constituents.

The variable compositions of the studied melt pockets can be attributed to the relatively coarse grain size (2–4 mm) of the host rock minerals compared to the diameters of the melt pockets (<4 mm). The melt pockets are not large enough to represent a bulk rock melt of Los Angeles. Instead, they represent localized, mineral-scale melting products. Melt pocket compositions, presented in Table 3, differ markedly when comparing those of the smaller melt pockets, Types 1 and 2, to the larger Type 3 melt pockets. Types 1 and 2 are enriched in SiO_2, Al_2O_3, and alkalis as compared to Type 3. The CIPW norm calculations, also listed in Table 3, indicate that the precursors of Types 1 and 2 melt pockets were mainly quartz + alkali feldspar + plagioclase + pyroxene, while those for Type 3 were mainly plagioclase + pyroxene + whitlockite. Therefore, the precursors of Types 1 and 2 melt pockets likely had a large contribution from late-stage minerals (mesostasis), while the bulk of Type 3 are derived from the main host rock lithology. This is not surprising considering that shock melting begins at grain boundary margins where mesostasis is more abundant. Thus, smaller (Type 1 and 2) melt pockets will posses a greater contribution of mesostasis to bulk composition than larger (Type 3) melt pockets that have melted approximately the same amount of mesostasis but greater proportions of host rock phases.

Based on compositional and textural lines of evidence, we conclude that the melt pockets formed by the local *in situ* melting of host rock minerals as opposed to forceful injection of extraneous impact melt along fractures in the host rock. Remobilization and injection of opaques and melt from the melt region into pre-existing fractures in adjacent host rock pyroxene could have occurred during compression and subsequent stress relaxation. The contact between the melt pockets and adjacent host minerals is intrusive in places. The intensity of shock features is observed to increase with proximity to the melt pockets, indicating a localized increase in shock pressure. This pressure gradient from melt pocket (60–80 GPa) to bulk rock (35–40 GPa) is certainly sufficient to account for forceful injection of Fe-sulfides and melt from the melt pockets into adjacent host minerals. Additionally, intrusions could have formed by pressure generated by a volume increase (~10%) associated with the melting event.

The relationship between areas of alkali- and silica-rich glass and the melt pockets is puzzling. However, comingling and entrapment of liquid blebs from the melt pocket is possible if the two phases were initially molten at the same time. This could be explained if the alkali- and silica-rich glass was formed during the shock event but was quenched before the shock pressure was completely released. Melt from the melt pocket could then have remained in a liquid state after pressure release. This is consistent with the presence of abundant vesicles in the melt pocket glasses, indicating low confining pressure. Stopler and McSween (1979) observed similar textural associations in Shergotty and Zagami, concluding that they may represent shock mixtures of alkali-feldspars and silica.

The presence of clasts in one melt pocket with quench textures, as well as the presence of crosscutting silicate melts, does not require multiple impact events. That a single impact event is capable of producing several shock metamorphic features in a target rock is well-documented (e.g., Stöffler 1984; Stöffler et al. 1991). The high concentration of relatively cold lithic and crystal fragments, as well as the proximity to the melt pocket margin, may have facilitated rapid crystallization of one melt with respect to the other. Rapid crystallization could also cause a drastic increase in the viscosity of one melt with respect to the other.

The development of abundant crystallites and glass in the melt pockets attests to rapid cooling of the melt, which implies that the studied Los Angeles samples were derived from the chilled margins of a larger ejected body (several meters to tens of meters in diameter) or were never much larger than the recovered meteorite sizes (tens of cm in diameter). The high abundance of relatively cold clasts in the smaller melt pockets (Type 1) probably contributed to the rapid crystallization (generating abundant crystallites) and an absence of flow textures, due to the presence of copious heterogeneous nucleation sites. Vesiculation probably occurred during shock decompression, with vesicles persisting in the melt under lower pressure conditions (Kenkmann et al. 2000). However, this does not preclude the development of high pressure, high temperature polymorphs within the melt pockets produced by cavitation and bubble implosion (Spray 1999). Melt veins and melt

dikelets occur in direct contact with the melt pockets and are considered morphologically distinct from typical "shock veins" that transect meteorites and that form by a combination of shock and frictional melting. The concentric zoning observed in the margins of clinopyroxenes in contact with melt pockets coincides with a progressive reduction in birefringence, which suggests that shock excursions were focused as point sources and that these were generated in the wake of the planar shock front that induced bulk shock effects. We infer that the larger melt pockets (Type 3) were formed by higher energy excursions relative to the smaller pockets (Type 1 and 2).

Based on experimental data by Kieffer et al. (1976), Schaal and Hörz (1977), and Schmitt (2000), shock pressure and temperature excursions of 60–80 GPa and 1600– 2000°C are estimated for Los Angeles 7058. Because pyroxene is not observed as clasts in any of the melt pockets in Los Angeles, the higher pressure of ~80 GPa is favored, coincident with the observed melting of pyroxene in experimentally shocked basalts (Schaal and Hörz 1977). These discrete excursions are, therefore, approximately twice the magnitude of the bulk shock (35–40 GPa).

A young formation age, 170 ± 8 Ma, for the Los Angeles meteorite (Nyquist et al. 2001) precludes it recording multiple impact events that would be more typical of target rocks from the older impact-scarred Noachian terrains of the southern hemisphere. Instead, Los Angeles records evidence of a single shock event, which favors its launching immediately following hypervelocity impact into a relatively young (late Amazonian) volcanic source terrain, such as is found in the Tharsis and Elysium regions.

Acknowledgments–This work has been funded by the Natural Sciences and Engineering Research Council of Canada (NSERC) through research grants awarded to J. G. Spray and an NSERC PGS-b scholarship awarded to E. L. Walton. We thank Tim McCoy at the Smithsonian Institution, Washington D.C., for loan of the samples; Douglas Hall at UNB and Michael Coy at JEOL USA for EM support, Cliff Shaw for helpful discussions, and Angel Gomez for drafting. Constructive Reviews by Y. Ikeda and R. F. Schmitt are gratefully acknowledged. Planetary and Space Science Centre Contribution 31.

Editorial Handling—Dr. Edward Scott

REFERENCES

Chen M. and El Goresy A. 2000. The nature of maskelynite in shocked meteorites: Not a diaplectic glass but a glass quenched from shock-induced dense melt at high pressures. *Earth and Planetary Science Letters* 179:489–502.

El Goresy A., Fechtig H., and Ottemann J. 1968. The opaque minerals in impact glasses. In *Shock metamorphism of natural materials,* edited by French B. M. and Short N. M. Baltimore: Mono Book. pp. 531–553.

Garrison D. H. and Bogard D. D. 2000. Cosmogenic and trapped noble gases in the Los Angeles meteorite (abstract). *Meteoritics & Planetary Science* 35:A58.

Hörz F. and Quaide W. L. 1973. Debye-Scherrer investigations of experimentally shocked silicates. *The Moon* 6:45–82.

Kenkmann T., Hornemann U., and Stöffler D. 2000. Experimental generation of shock-induced pseudotachylytes along lithological interfaces. *Meteoritics & Planetary Science* 35: 1275–1290.

Kieffer S. W., Schaal R. B., Gibbons R., Hörz F., Milton D. J., and Dube A. 1976. Shocked basalt from Lonar crater, India, and experimental analogues. Proceedings, 7th Lunar and Planetary Science Conference. pp. 1391–1412.

Kirkpatrick R. J. 1975. Crystal growth from the melt: A review. *American Mineralogist* 60:798–814.

Langenhorst F., Poirier J. P., Deutsch A., and Hornemann U. 2002. Experimental approach to generate shock veins in single crystal olivine by shear melting. *Meteoritics & Planetary Science* 37: 1541–1553.

McSween H. Y., Jr. 2002. The rocks of Mars, from far and near. *Meteoritics & Planetary Science* 37:7–25.

Melosh H. J. 1984. Impact ejection, spallation, and the origin of meteorites. *Icarus* 59:234–260.

Melosh H. J. 1985. Ejection of rock fragments from planetary bodies. *Geology* 13:144–148.

Nishiizumi K., Caffee M. W., and Masarik J. 2000. Cosmogenic radiocunclides in Los Angeles martian meteorite (abstract). *Meteoritics & Planetary Science* 35:A120.

Nyquist L. E., Reese Y. D., Wiesmann H., Shih C. Y., and Schwandt C. 2000. Rubidium-strontium age of the Los Angeles shergottite. *Meteoritics & Planetary Science* 35:A121–A122.

Nyquist L. E., Bogard D. D., Shih C. Y., Greshake A., Stöffler D., and Eugster O. 2001. Ages and histories of martian meteorites. *Chronology and Evolution of Mars* 96:105–164.

Rubin A. E., Warren P. H., Greenwood J. P., Verish R. S., Leshin L. A., Hervig R. L., and Clayton R. N. 2000. Los Angeles: The most differentiated basaltic martian meteorites. *Geology* 28:1011–1014.

Schaal R. B. and Hörz F. 1977. Shock metamorphism of lunar and terrestrial basalts. Proceedings, 8th Lunar and Planetary Science Conference. pp. 1679–1729.

Schmitt R. T. 2000. Shock experiments with the H6 chondrite Kernouvé: Pressure calibration of microscopic shock effects. *Meteoritics & Planetary Science* 3:545–560.

Spray J. G. 1999. Shocking rocks by cavitation and bubble implosion. *Geology* 27:695–698.

Spray J. G. and Rae D. A. 1995. Quantitative electron-microprobe analysis of alkali silicate glasses: A review and user guide. *Canadian Mineralogist* 33:323–332.

Stöffler D. 1984. Glasses formed by hypervelocity impact. *Journal of Non-Crystalline Solids* 67:465–502.

Stöffler D. 2000. Maskelynite confirmed as diaplectic glass: Indications for peak shock pressure below 45 GPa in all martian meteorites (abstract #1170). 31st Lunar and Planetary Science Conference. CD-ROM.

Stöffler D., Ostertag R., Jammes C., and Pfannschmidt G. 1986. Shock metamorphism and petrography of the Shergotty achondrite. *Geochimica et Cosmochimica Acta* 50:889–903.

Stöffler D., Keil K., and Scott E. R. D. 1991. Shock metamorphism of ordinary chondrites. *Geochimica et Cosmochimica Acta* 5: 3845–3867.

Stopler E. and McSween H. Y., Jr. 1979. Petrology and origin of the shergottite meteorites. *Geochimica et Cosmochimica Acta* 43: 1475–1498.

Terribilini D., Busemann H., and Eugster O. 2000. Krypton-81-

krypton cosmic ray exposure ages of martian meteorites including the new shergottite Los Angeles (abstract). *Meteoritics & Planetary Science* 35:A155–A156.

Warren P. H., Greenwood J. P., Richardson J. W., Rubin A. E., and Verish R. S. 2000. Geochemistry of Los Angeles; A ferroan, La- and Th-rich basalt from Mars (abstract #2001). 31st Lunar and Planetary Science Conference. CD-ROM.

Xirouchakis D., Draper D. S., Schwandt C. S., and Lanzirotti A. 2002. Crystallization of Los Angeles, a basaltic martian meteorite. *Geochimica et Cosmochimica Acta* 66:1867–1880.